Texture-Induced Modulations of Friction Force: The Fingerprint Effect

E. Wandersman, R. Candelier, G. Debrégeas, and A. Prevost*

Laboratoire Jean Perrin, Ecole Normale Supérieure, UPMC Université Paris 6, CNRS FRE 3231, 24 rue Lhomond, 75005 Paris, France

(Received 13 July 2011; published 11 October 2011)

Modulations of the friction force in dry solid friction are usually attributed to macroscopic stick-slip instabilities. Here we show that a distinct, quasistatic mechanism can also lead to nearly periodic force oscillations during sliding contact between an elastomer patterned with parallel grooves, and abraded glass slides. The dominant oscillation frequency is set by the ratio between the sliding velocity and the grooves period. A model is derived which quantitatively captures the dependence of the force modulations amplitude with the normal load, the grooves period, and the slides roughness characteristics. The model's main ingredient is the nonlinearity of the friction law. Since such nonlinearity is ubiquitous for soft solids, this ''fingerprint effect'' should be relevant to a large class of frictional configurations and have important consequences in human digital touch.

DOI: 10.1103/PhysRevLett.107.164301 PACS numbers: 46.55.+d, 68.35.Ct, 81.40.Pq

Surface texture engineering by nano- or micropatterning techniques has proven to be an efficient tool to tune frictional or adhesive properties at solid-solid [1–3] or solid-liquid interfaces [4]. Many of the existing designs are directly inspired by natural surfaces. Superhydrophobic surfaces, for example, reproduce the microscopic pattern observed on lotus flower leaves [5]. Surfaces with a shark skinlike texture provide significant drag reduction in turbulent flows [6]. Geckos feet fibrillar structure provides them with remarkable adhesion capabilities, and has allowed the design of functional adhesives [7].

In comparison, the effect of micropatterning in solid-solid friction has so far attracted much less attention. In a recent paper however, we suggested that epidermal ridges—the regular pattern characteristics of humans and primates glabrous skin surface—strongly modify the skin internal stress elicited upon actively rubbing the fingertip over a finely abraded surface, thus enhancing tactile sensitivity [8]. More precisely, such patterns were shown to produce a nearly periodic modulation of the texture-induced subcutaneous stress field at a frequency set by the ratio between the scanning velocity and the pattern period. This finding led to the integration of fingerprintlike structures in several robotic hand designs [9,10]. Interestingly, this effect not only shows up in local stress measurements but is also observed in the global friction force signal measured while scanning a human finger on a rough surface [11]. Since the friction force signal conveys a large part of the tactile information for texture discrimination, as recently evidenced in psychophysical assays [12], it is crucial from both biological and robotic points of views to understand the physical origin of such texture-induced friction force modulations and to identify the parameters which control their spectral characteristics.

To address this question, we investigate in this Letter the friction dynamics between a patterned elastomer block and a finely abraded glass surface in a sphere-on-plane geometry (Fig. 1). The elastomer blocks (thickness ≈ 18 mm) were obtained by molding liquid polydimethylsiloxane–cross-linker mixture (PDMS, Sylgard 184, Dow Corning) in concave spherical lenses of radius of curvature $R = 128.8$ mm. Prior to molding, the surface of the lenses was patterned with a periodic square grating of depth 40 μm and spatial period $\lambda = 125$, 218, or 760 μm (width $\lambda/2$) using soft photolithography techniques [8]. The elastomer Young's modulus was measured to be $E = 2.2 \pm 0.1$ MPa. The abraded planes consisted in microscope glass slides sandblasted or abraded using a silicon carbide powder-water mixture. The surface topography was measured with an optical profilometer (M3D, Fogale Nanotech) from which the root mean-squared height h_{rms} and surface profile autocorrelation spectrum $C(q)$ were computed [13]. Two substrates were considered, referred to as ''rough-'' ($h_{\mathrm{rms}} \approx 2.3$ μm) and ''rough+'' ($h_{\mathrm{rms}} \approx 5$ μm), respectively. For both, $C(q)$ displays a self-affine behavior as usually observed for real surfaces [14] of the form $C(q) = C_0[1 + (q/q_c)^2]^{-\alpha}$ with $(C_0, q_c, \alpha) = (1.310^{-22}\ \mathrm{m}^4, 610^4\ \mathrm{m}^{-1}, 1.29)$ and $(1.310^{-20}\ \mathrm{m}^4, 8.510^3\ \mathrm{m}^{-1}, 1.32)$ for substrate rough- and rough+, respectively. Substrates were rubbed against the elastomer surface along the x direction at constant velocity v (range 0.01–0.5 mm s^{-1}) with a motorized translation stage (LTA-HL, Newport), under constant normal force F_N (range 0.02–2 N). F_N and tangential force F_S were measured with a 1 mN accuracy at 1 kHz by monitoring the deflections of two orthogonal cantilevers (Fig. 1, normal and tangential stiffness respectively 733 ± 3 Nm^{-1} and 9743 ± 47 Nm^{-1}) using capacitive position sensors (MCC-20 and MCC-10, Fogale Nanotech). The apparent contact zone, imaged in a light-transmitted geometry (Fig. 1) had a diameter ranging from 1 to 6 mm (a few λ to about 50λ), much larger than the substrate roughness characteristic scale.

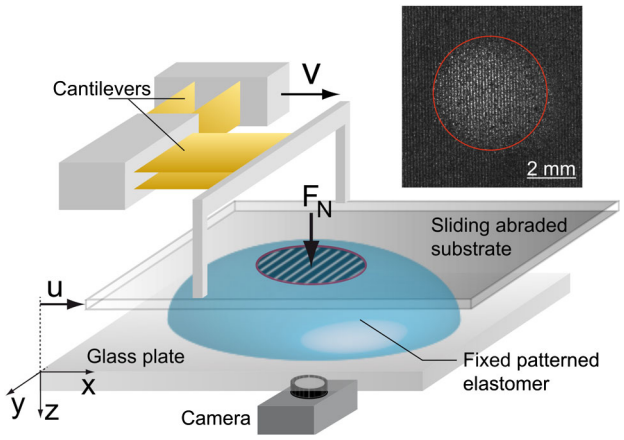

FIG. 1 (color online). Sketch of the setup. Inset: image of a typical contact at $F_N = 0.5$ N with $\lambda = 125$ μm. The red circle defines the apparent contact perimeter.

Typical F_S signals in steady sliding are shown on Figs. 2(a)–2(d) as a function of the scanned distance $u = v.t$ with $v = 0.1$ mm s^{-1} perpendicular to the direction of the ridges and $F_N = 0.5$ N. Minute but clearly measurable nearly periodic oscillations are observed, with no equivalent in the normal force signals. Their amplitude weakly depends on λ and increases with F_N. They are significantly more pronounced with the rough+ than with the rough- substrate [Figs. 2(b) and 2(d)]. The effect entirely vanishes when the direction of the ridges is aligned with the direction of motion. In the range of velocities explored, these modulations are independent of v. All experiments presented further are thus done at $v = 0.1$ mm s^{-1} and u is taken as the time-varying variable.

The power spectrum $S_{[\delta F_S]}(q)$ of $\delta F_S(u) = F_S(u) - \bar{F}_S$ (the bar stands for time averaging) was computed by averaging over a 20 mm travel distance. All spectra exhibit well-defined peaks at $q_\lambda = 2\pi/\lambda$ and at corresponding harmonics [Fig. 2(e)]. $S_{[\delta F_S]}$ at $q = q_\lambda$ increases with F_N as AF_N^ν (Fig. 3) where values of A and ν are collected in Table I. As mentioned above, A depends weakly on λ and is significantly higher for the rough+ than for the rough- substrate. The exponent ν is close to 1 for all experimental configurations.

In parallel to the force measurements, rapid imaging of the contact zone was performed using a fast camera (Fastcam APX-RS, Photron, Japan) operating at 60 Hz. At all loads, contact occurs only at the summits of the ridges, thus yielding a large contrast between the top and bottom of the pattern and allowing for a precise tracking of the edges of the ridges with ≈ 10 μm accuracy. No stick-slip motion of the ridges was observed. Thus, the measured force oscillations cannot be accounted for by periodic stick-slip events whose frequency is set by the period of the pattern as reported in [2]. This is further supported by the observation that the fluctuations are quasistatic (v independent).

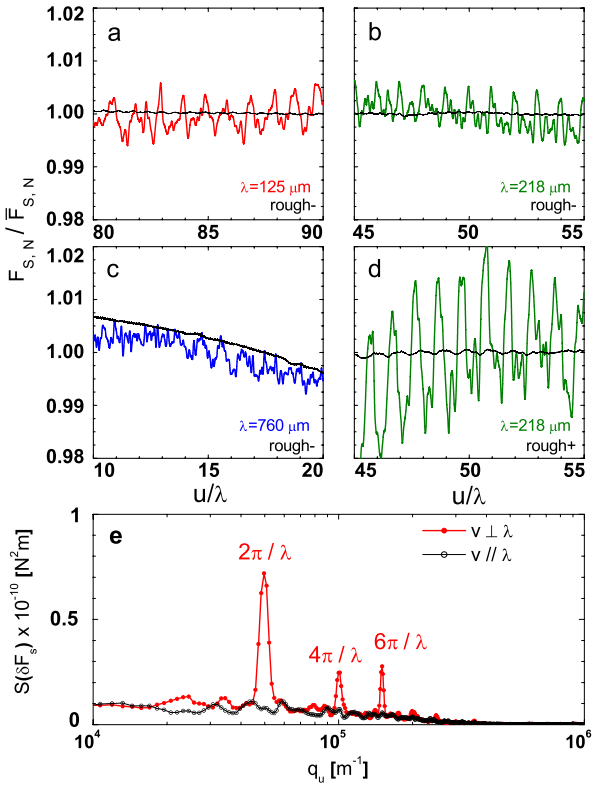

FIG. 2 (color online). (a)–(d) Blow up of $F_S/\bar{F}_S$ fluctuations ($F_N/\bar{F}_N$ in thin black lines) versus u/λ at $F_N = 0.5$ N for different λ and both substrates in steady sliding. (e) Averaged power spectra of F_S fluctuations ($\lambda = 125$ μm, $F_N = 0.5$ N, "rough-" substrate), both with v perpendicular (●) and parallel (○) to the ridges.

In the rest of this Letter, we aim at understanding the physical origin of the observed friction force modulation and the dependence of its amplitude with the normal load, pattern period, and substrate roughness characteristics. We first consider a perfectly smooth elastomer surface (no patterning) rubbed against an abraded glass slide. We denote $p(x, y, u)$ and $\tau(x, y, u)$ the normal and tangential stress field at a given position u of the substrate, such that $F_N(u) = \int p(x, y, u)dxdy$ and $F_S(u) = \int \tau(x, y, u)dxdy$. Under a local Amontons-Coulomb friction law assumption, i.e., $\tau(x, y, u) = \mu_0 p(x, y, u)$ with μ_0 a uniform (material dependent) friction coefficient, the friction force reads $F_S(u) = \mu_0 F_N$ and is thus expected to be time independent. We therefore hypothesize a weakly nonlinear relationship between $p(x, y, u)$ and $\tau(x, y, u)$ which is equivalent to postulating a pressure dependence of the local friction coefficient, i.e., $\mu = \tau/p = \mu(p)$. The friction force now reads

$$F_S(u) = \int \mu(p)p(x, y, u)dxdy. \quad (1)$$

The spatial variations of $p(x, y, u)$ can be decomposed into a time-averaged component $\bar{p}(x, y)$ set by the macroscale

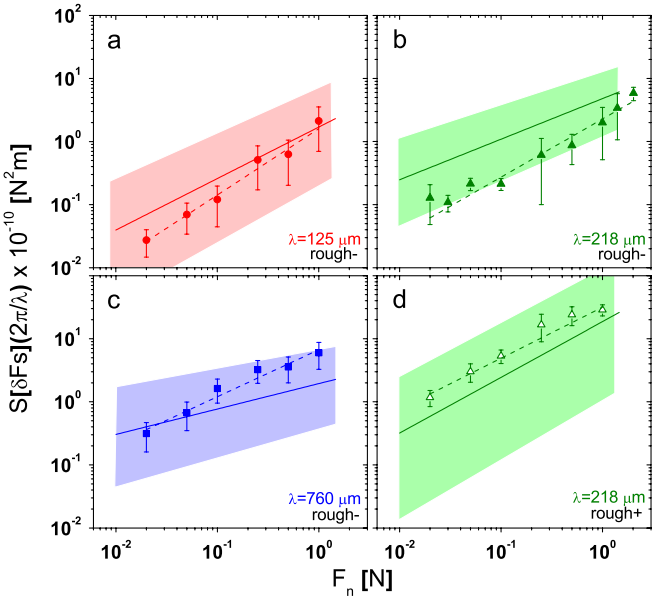

FIG. 3 (color online). (a)–(d) $S_{[\delta F_S]}(q_\lambda)$ versus F_N. Dashed lines are best experimental fits, solid lines are model predictions. Shaded areas bound the values of A by tuning the parameters of the model within their experimental errors.

plane-on-sphere contact geometry and a time-fluctuating component $\delta p(x, y, u)$ associated with the microscopic roughness of the glass slide. For simplicity, we further assume that the elastomer is in intimate contact with the glass surface. This assumption is expected to fail at the microasperities scale but should be valid at intermediate scale such as the interridge distance λ. In this limit, the texture-induced pressure modulations are set by the topography of the glass substrate and are independent of the local mean pressure imposed by the Hertzian geometry $\bar{p}(x, y)$. The pressure modulation field $\delta p(x, y, u)$ is thus a sole function of the position of the substrate with respect to the contact zone $(u - x, y)$, so that the pressure field reads

$$p(x, y, u) = K(u)[\bar{p}(x, y) + \delta p(u - x, y)]. \quad (2)$$

The normalization factor $K(u)$ ensures that F_N remains constant during sliding. This condition imposes

TABLE I. Experimental and model parameters with $A \times 10^{-10}$ given in SI units.

Configuration	A^{exp}	ν^{exp}	A^{model}	ν^{model}
$\lambda = 125$ μm, rough−	1.6 ± 0.9	1.1 ± 0.3	1.7	0.87
$\lambda = 218$ μm, rough−	2.3 ± 0.5	0.9 ± 0.1	4.8	0.64
$\lambda = 218$ μm, rough+	32 ± 4	0.8 ± 0.15	19	0.88
$\lambda = 760$ μm, rough−	7 ± 2	0.8 ± 0.2	2.0	0.4

$$K(u) = \left(1 + \frac{1}{F_N}\int \delta p(u - x, y)dxdy\right)^{-1} \approx 1 - \frac{1}{F_N}\int \delta p(u - x, y)dxdy. \quad (3)$$

The latter expansion is valid when the contact diameter is much larger than the texture scale. Indeed, in this limit, the integral of the roughness-induced pressure field becomes vanishingly small with respect to the confining force F_N. Rewriting Eq. (1), one obtains

$$\delta F_s(u) = F_s(u) - \bar{F}_s = \int[\mu(\bar{p}) - \langle\mu\rangle]\delta p(u - x, y)dxdy,$$

where $\langle\mu\rangle$ is defined as the ratio $\bar{F}_S/F_N$.

The friction force fluctuations thus appear as the convolution product of a function characterizing the friction coefficient spatial heterogeneities and the texture-induced pressure modulations field. The presence of regular ridges at the surface of the elastomer imposes that the stress between ridges vanishes. This can be accounted for, in first approximation, by introducing a λ-periodic Heavyside function $H(x) = \theta[\sin(2\pi x/\lambda)]$ under the integral, which directly results in a spectral selection of the associated spatial mode.

In Fourier space [13], the fluctuating component of the friction force thus reads

$$S_{[\delta F_S]}(q_u) = (2\pi)^4 \int dq_v |\mathcal{F}(H(x)[\mu(x, y) - \langle\mu\rangle])|^2 S_{[\delta p]}.$$

Wave vector q_u (q_v) refers to the parallel (perpendicular) direction to the sliding direction.

Under the assumption of intimate contact, $S_{[\delta p]}$ can be simply expressed as a function of the roughness spectrum $C(q)$ [13] as $S_{[\delta p]}(q) = (E^*/2)^2 q^2 C(q)$, where q is the norm of (q_u, q_v) and E^* the reduced Young's modulus. Lacking any established constitutive law for our system, the friction coefficient spatial field, on the other hand, is estimated empirically from global force measurements. For all experimental configurations, a power-law dependence is observed between both force components $\bar{F}_S = B.F_N^\gamma$ with $\gamma = 0.87 \pm 0.04$ (Fig. 4). We postulate a power-law relationship between the local shear stress and the local pressure $\tau(x, y) = \beta\bar{p}^m(x, y)$ [15]. Assuming that $\bar{p}(x, y)$ follows a Hertz profile, $\bar{F}_S$ can be derived by analytically integrating $\tau(x, y)$ over the contact area, yielding $\gamma = (m + 2)/3$ and an exact relationship between β, B, and γ. Figure 4 shows a comparison between $\bar{F}_S$ versus F_N obtained experimentally and through integration of τ over the contact area. Note that the choice of a power law is simply dictated by the fact that it constitutes the simplest functional form consistent with the global force measurements in the explored range.

Both predicted and measured amplitudes of $S_{[\delta F_S]}(q_\lambda)$ with F_N are presented on Fig. 3, for all experimental

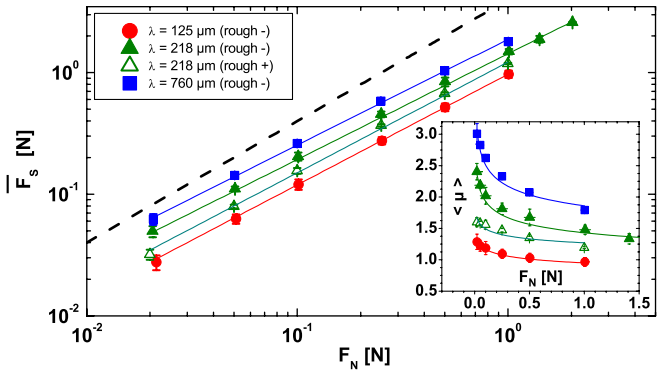

FIG. 4 (color online). Time-averaged friction force $\bar{F}_s$ versus F_N. Different symbols correspond to different configurations. Solid lines are power-law fits with exponent γ. Combined fits yield $\gamma = 0.87 \pm 0.04$. The dashed line has a slope of 1. Inset: Average dynamic friction coefficient $\bar{F}_S/F_N$ versus F_N. Solid lines are power-law fits with exponent $\gamma - 1$.

configurations, using the set of parameters (β, m, C_0, q_c, α) obtained as described earlier. Using the mean values of these parameters, the predicted amplitude of F_S modulations is in reasonable agreement with the data, without any adjustable parameter (solid lines on Fig. 3). The model captures, in particular, the analytic increase of $S_{[\delta F_s]}(q_\lambda)$ with F_N, with an exponent ν comparable to its experimental counterpart (see Table I and Fig. 3). For all λ we determined the boundaries on $S_{[\delta F_S]}(q_\lambda)$ based on the experimental uncertainties of the parameters (shaded areas on Fig. 3). The large uncertainty on A and ν (~ 0.1) in the model is mostly due to the experimental inaccuracy in evaluating the parameter m. Exploring the model predictions beyond the range of the experimental parameters reveals that ν increases linearly with m and decreases linearly with λ in the investigated range (not shown). The predicted amplitude A is trivially proportional to C_0, slightly decreases with λ, and falls rapidly to zero when m approaches unity, i.e., when Amontons-Coulomb friction's law is assumed locally.

This study shows that any nonlinearity in the friction law leads to the development of texture-induced friction force fluctuations. Since purely linear friction laws are scarcely observed, the present mechanism should be relevant to most practical situations. More generally, whenever the local and global friction coefficients are not the same [16] force fluctuations should occur. However, these are expected to be in practice hardly detectable when the fixed substrate (here the PDMS block) is smooth and the contact zone diameter is much larger than the typical roughness scale. In contrast, the presence of a regular pattern at the surface of the block operates a spectral filtering of the texture-induced pressure modulation which induces a mode selection of the force fluctuations at a particular frequency. The amplitude of these force fluctuations can then become an order of magnitude larger than in the smooth case as shown by the present study. This mechanism was here examined for the simplest possible pattern, i.e., regular parallel stripes, but richer force signal spectra should be similarly obtained with more complex patterns.

In essence, the macroscopic friction force signal carries information about the spectral content of the microscopic substrate topography at frequencies defined by the elastomer micropattern. A practical consequence is that F_S fluctuations amplitudes could be used to discriminate surfaces having small differences in their roughness at scales much smaller than the contact extension. Hence, under the same conditions, force fluctuations are roughly 10 times larger for the substrate having a $h_{\mathrm{rms}} \approx 5$ μm than for the one with $h_{\mathrm{rms}} \approx 2.3$ μm. This mechanism could also facilitate the detection of motion. The transition between static and sliding contact should manifest as the sudden appearance of large single mode oscillations of the friction force. One may finally foresee the possibility to evaluate the scanning velocity, based on the sole friction force signal, by continuously extracting the peak frequency of these oscillations. We believe that this "spectrotribometry" approach may be relevant to human digital touch and prehension, owing to the presence of fingerprints, and that it could be easily implemented in tactile robotic sensing devices.

The authors deeply thank F. Petrellis for illuminating mathematical surgery, F. Zalamea for his valuable help, A. Chateauminois and C. Frétigny for fruitful discussions, and acknowledge financial support from ANR-DYNALO NT09-499845.

*alexis.prevost@lps.ens.fr

[1] C. J. Rand and A. J. Crosby, J. Appl. Phys. **106**, 064913 (2009).
[2] R. Bennewitz *et al.*, J. Phys. Condens. Matter **20**, 015004 (2008).
[3] F. Wu-Bavouzet, J. Cayer-Barrioz, A. Le Bot, F. Brochard-Wyart, and A. Buguin, Phys. Rev. E **82**, 031806 (2010).
[4] P. Joseph *et al.*, Phys. Rev. Lett. **97**, 156104 (2006).
[5] B. Bhushan, Y. C. Jung, and K. Koch, Phil. Trans. R. Soc. A **367**, 1631 (2009).
[6] B. Dean and B. Bhushan, Phil. Trans. R. Soc. A **368**, 4775 (2010).
[7] L. F. Boesel, C. Greiner, E. Artz, and A. del Campo, Adv. Mater. **22**, 2125 (2010).
[8] J. Scheibert, S. Leurent, A. Prevost, and G. Debrégeas, Science **323**, 1503 (2009).
[9] Y. Zhang, J. Micromech. Microeng. **20**, 085012 (2010).
[10] D. D. Damian, H. Martinez, K. Dermitzakis, A. Hernandez-Arieta, and R. Pfeifer, in *Proceedings of the International Conference on Intelligent Robots and Systems* (IEEE, New York, 2010), p. 904.

[11] A. Prevost, J. Scheibert, and G. Debrégeas, Comm. Int. Biol. **2**, 422 (2009).
[12] M. Wiertlewski, J. Lozada, and V. Hayward, IEEE. Trans. Robot. **27**, 461 (2011).
[13] B. N. J. Persson, J. Phys. Condens. Matter **20**, 312001 (2008).
[14] B. N. J. Persson, J. Chem. Phys. **115**, 3840 (2001).
[15] C. H. Scholz, *The Mechanics of Earthquakes and Faulting* (Cambridge University Press, Cambridge, U.K., 2010).
[16] O. Ben-David and J. Fineberg, Phys. Rev. Lett. **106**, 254301 (2011).